Neuron, Vol. 31, 929–941, September 27, 2001, Copyright ©2001 by Cell Press

The Reelin Pathway Modulates the Structure and Function of Retinal Synaptic Circuitry

Dennis S. Rice,[1,5] Steve Nusinowitz,[2] Asif M. Azimi,[2] Albert Martínez,[3] Eduardo Soriano,[3] and Tom Curran[1,4]

[1] Department of Developmental Neurobiology
St. Jude Children's Research Hospital
Memphis, Tennessee 38105

[2] The Jules Stein Eye Institute
UCLA School of Medicine
Los Angeles, California 90095

[3] Department of Cell Biology and Neuroscience
Research Center (CERN)
University of Barcelona
08028 Barcelona
Spain

Summary

The formation of synaptic connections requires the coordination of specific guidance molecules and spontaneous neuronal activity. The visual system has provided a useful model for understanding the role of these cues in shaping the precise connections from the neural retina to the brain. Here, we demonstrate that two essential genes in the Reelin signaling pathway function during the patterning of synaptic connectivity in the retina. Physiological studies of mice deficient in either *reelin* or *disabled-1* reveal an attenuation of rod-driven retinal responses. This defect is associated with a decrease in rod bipolar cell density and an abnormal distribution of processes in the inner plexiform layer . These results imply that, in addition to its essential role during neuronal migration, the Reelin pathway contributes to the formation of neuronal circuits in the central nervous system.

Introduction

The identification and characterization of neurological mutant mice has identified a signaling pathway required for appropriate cell positioning in the developing nervous system. The first gene to be identified in this pathway, *reelin*, is disrupted in the classical neurological mutant mouse, *reeler* (D'Arcangelo et al., 1995). Recently, mutations in *reelin* have also been associated with autosomal lissencephaly in humans (Hong et al., 2000). Reelin is a secreted protein produced by distinct cell types in the developing brain, including Cajal-Retzius cells in the cerebral cortex and hippocampus and granule cells in the cerebellum (D'Arcangelo et al., 1995; Ogawa et al., 1995). Anatomical studies in *reeler* mice demonstrated a failure in cell positioning in the developing brain (Caviness and Rakic, 1978; Goffinet, 1984). For example, in the developing cerebral cortex, neurons migrate into a structure known as the preplate, containing high levels of Reelin secreted by Cajal-Retzius cells. In *reeler*, migrating neurons fail to invade the preplate and instead they accumulate beneath in a disorganized cortical plate (Hoffarth et al., 1995; Ogawa et al., 1995; Sheppard and Pearlman, 1997).

Reelin binds to the Very low-density lipoprotein receptor (Vldlr) and the Apolipoprotein E Receptor-2 (ApoER2) that are expressed on migrating neurons (D'Arcangelo et al., 1999; Hiesberger et al., 1999). The cytoplasmic domains of these receptors contain a NPxY motif that binds to a protein interaction domain in Disabled-1 (Dab1), an adaptor protein present primarily in the brain (Howell et al., 1997a; Trommsdorff et al., 1999). Mice lacking both *vldlr* and *apoER2* exhibit ataxia and identical disruptions in neuronal positioning to those in *reelin*- or *dab1*-deficient mice (D'Arcangelo et al., 1995; Howell et al., 1997b; Sheldon et al., 1997; Trommsdorff et al., 1999). The interaction of Reelin with lipoprotein receptors on embryonic neurons stimulates phosphorylation of Dab1 on tyrosine residues (Howell et al., 1999; Keshvara et al., 2001). Mice in which these tyrosines are replaced with phenylalanine exhibit *reeler*-like characteristics, implying that a Reelin-activated kinase signaling pathway is important for cell positioning in the brain (Howell et al., 2000). Moreover, Dab1 levels are dramatically elevated in the neurons that go astray in *reeler* brains and those deficient in both *vldlr* and *apoER2* (Rice et al., 1998; Trommsdorff et al., 1999). Taken together, the genetic and biochemical data support a critical role for Dab1 as a downstream component of a signal transduction pathway that enables migrating neurons to reach their final destinations in laminated brain regions such as the cerebral cortex, hippocampus, and cerebellum.

Reelin, *vldlr*, *apoER2*, and *dab1* continue to be expressed following neuronal migration, although the function of the Reelin pathway in postnatal and adult brain is not known (Alcantara et al., 1998; Kim et al., 1996; Rice et al., 1998). Some suggestions have been made based on careful studies indicating that Reelin contributes to the guidance mechanisms controlling the formation of hippocampal projections (Del Rio et al., 1997; Borrell et al., 1999). Furthermore, a number of factors linked to neurodegeneration have been associated with the Reelin pathway during development (D'Arcangelo et al., 1999; Hiesberger et al., 1999). Indeed, analysis of Reelin expression levels suggested a potential role for Reelin in the pathogenesis of neuropsychosis (Fatemi et al., 2000; Guidotti et al., 2000). However, at present there is no clear support for a function of the Reelin pathway in events other than those controlling cell positioning in the developing brain.

The mammalian retina is organized into three cell layers and two synaptic layers. Rod and cone photoreceptors are located in the outer nuclear layer (ONL). Horizontal, bipolar, amacrine, and Müller cells are contained within the inner nuclear layer (INL). Retinal ganglion cells and a subset of amacrine cells are located in the ganglion cell layer (GCL). Retinal cells arise in an overlapping but coordinated fashion from a ventricular zone that lines the back of the eye (Lillien, 1994). Unlike other

[4] Correspondence: fos1@aol.com

[5] Present address: Lexicon Genetics, Inc., 4000 Research Forest Drive, The Woodlands, Texas 77381.

laminated brain regions, there is no relationship between the final laminar position of a retinal cell and its time of origin. For example, ganglion, horizontal, amacrine, and cone cells arise first, followed by bipolar neurons and Müller glia. Rod photoreceptors are produced throughout retinal histogenesis (Young, 1985).

The retina exhibits a normal cellular organization in *reeler* mice, although *reelin* is normally present at high levels in the GCL during embryonic and postnatal development (Schiffmann et al., 1997). Therefore, the retina provides an ideal model system in which to address additional biological functions of the Reelin pathway. Indeed, we have shown that Dab1 is first detectable in mouse retina after birth and it persists primarily in type AII amacrine cells, which are key interneurons in the scotopic synaptic circuitry (Rice and Curran, 2000). The present work examines the stratification patterns of type AII amacrine and rod bipolar processes in the inner plexiform (IPL), while comparing the density of these important interneurons in control mice and those lacking either *reelin* or *dab1*. Physiological responses in mice deficient in the Reelin pathway were determined using electroretinography (ERG). These results suggest that, in addition to its essential role during neuronal migration, the Reelin pathway contributes to the proper patterning of synaptic connectivity.

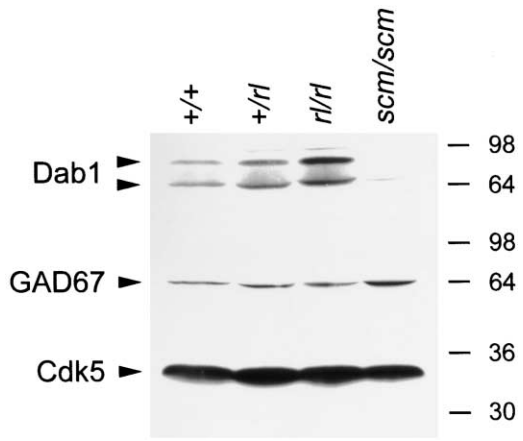

Figure 1. Immunoblot Analysis of Dab1 in Adult Eyes

The levels of Dab1 are elevated in *reeler* (*rl/rl*) compared with normal (+/+) or heterozygous (+/−) mice. *Scrambler* mice (*scm/scm*) contain low levels of Dab1 (Sheldon et al., 1997). Protein loading was similar among the groups as revealed with immunoblotting the same membrane with either Gad67 or Cdk5 antibodies. The molecular mass is indicated to the right.

Results

The Reelin Pathway Is Active in the Eye

Neurons in the *reeler* forebrain and cerebellum, which normally respond to Reelin, contain 5- to 10-fold more Dab1 than those in normal brain (Rice et al., 1998). Dab1 also accumulates in neurons obtained from mice lacking Reelin receptors, *vldlr* and *apoer2* (Trommsdorff et al., 1999). Recently, we found that Dab1 is expressed in glycinergic, type AII amacrine cells in the mouse retina (Rice and Curran, 2000). These important interneurons extend processes in two distinct strata of the inner plexiform layer (IPL), where they integrate into the On and Off physiological channels (Strettoi et al., 1992). Several isoforms of Dab1 were detected in immunoblotting assays using extracts obtained from adult eyes (Figure 1). Levels of all isoforms of Dab1 were elevated approximately 5- to 10-fold in *reeler* eyes compared to those from normal or heterozygous mice. These results demonstrate that the Reelin pathway is active in retina.

Reelin and Dab1 Are Expressed in Adjacent Cell Layers in the Retina

Immunohistochemical staining for Reelin and Dab1 was used to compare the distribution of these proteins at postnatal day 7. High levels of Reelin were detected in projections throughout the IPL (Figure 2A). Reelin was present in ganglion cells in the ganglion cell layer (GCL) and amacrine cells in the inner nuclear layer (INL). A subpopulation of developing bipolar neurons in the INL also contained Reelin. *Reeler* mice failed to show specific staining, but blood vessels were visible with the anti-mouse secondary (asterisks in Figure 2B). The same sections were labeled with Dab1 antibodies, which revealed elongated cells that may represent bipolar cells (Figure 2C). The highest levels of Dab1 were detected in the developing type AII amacrine cells and their projections in the IPL (arrowheads in Figure 2C). A dense network of processes containing Dab1 was located near the border of the IPL and the GCL (double arrows in Figure 2C), although the bistratification of type AII amacrine cell projections is not yet apparent at this age. Type AII cells were present at comparable locations in *reeler* retina and they extended projections into the IPL. However, this network of type AII amacrine cell processes was not apparent in *reeler* retinas at P7 (Figure 2D). In control retina, neurites containing Dab1 encountered Reelin during the time at which they elaborate projections into the IPL (Figure 2E). In the absence of Reelin, neurites containing Dab1 extended into the IPL, but their distribution was more uniform compared to that in control tissue (Figure 2F).

Intense Reelin immunostaining was observed in adult retinas, including cells in the GCL and INL (Figure 3A). High levels of Reelin were detected in the On sublamina of the IPL, which may represent dendrites of On retinal ganglion cells (Figure 3A). In the INL, Reelin was detected in a subset of amacrine cells (asterisk in Figure 3A) and in a subset of bipolar neurons (arrows in Figure 3A). The dendrites of these bipolar neurons invaded the outer plexiform layer (OPL). Retinas obtained from *reeler* mice failed to show specific staining with the Reelin antibody (Figure 3B). In contrast to Reelin, Dab1 expression in the adult retina was restricted to a single retinal cell class, type AII amacrine cells (Figure 3C). Projections from these cells distributed into the Off and On sublayers in the IPL (arrows in Figure 3C). In *reeler* retinas, type AII amacrine cells were located in the appropriate INL region (Figure 3D). However, the patterning of type AII amacrine cell projections in the IPL appeared less precise in *reeler* mice compared to that in controls (Figure 3D). Dab1 colocalized with Reelin in the On sublamina of the IPL in control mice (Figure 3E). In *reeler* retinas, projections that originate from type AII amacrine

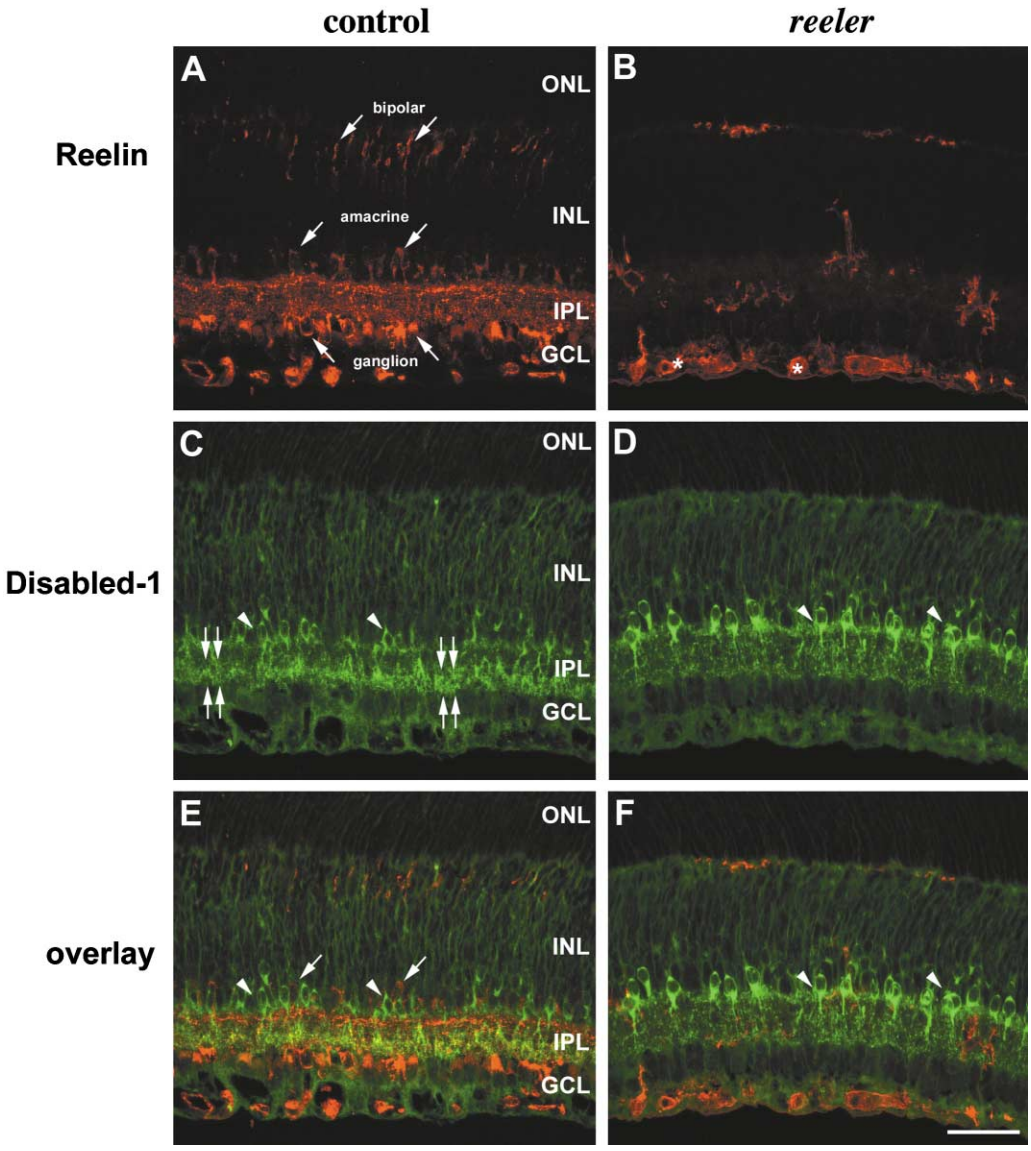

Figure 2. Distribution of Reelin and Dab1 in the Retina at Postnatal Day 7 in Control and *reeler* Retinas

(A) Reelin is present in the ganglion cell layer (GCL) and in the inner plexiform layer (IPL). Cell bodies and dendrites of retinal ganglion cells contain Reelin. A subset of amacrine cells and bipolar cells located in the inner nuclear layer (INL) also contains Reelin. (B) *Reeler* mice do not exhibit any specific staining with Reelin antibodies. The asterisks indicate blood vessels that crossreact with the secondary antibody. (C) Low levels of Dab1 are present throughout the INL, indicating that Dab1 is expressed in interneurons. Dab1 is expressed at high levels in type AII amacrine cells (arrowheads) located in the INL. Their projections extend in the IPL toward the GCL, where they form a dense network of projections (double arrows). (D) Type AII amacrine cells (arrowheads) are located in the correct cell layer in *reeler* retinas, indicating that Reelin is not required for cell positioning in retina. (E) Neurites containing Dab1 (green) in control retinas encounter Reelin (red) in the IPL. Their projections form a dense network near the GCL. Note that the amacrine cells expressing Dab1 (arrowheads) do not express Reelin (arrows). (F) The projections of type AII amacrine cells fail to form network near the GCL in the absence of Reelin. The scale bar in (F) is 50 μm.

cells were more broadly distributed throughout the IPL (Figure 3F).

The Reelin Pathway Modulates the Stratification Pattern of Retinal Interneuronal Projections within the IPL

Electron microscopy was used to compare the distribution of synaptic endings originating from type AII amacrine cells in control and *reeler* retinas. Two different types of endings located in five, equally thick sublayers of the IPL, known as S1–S5, were identified based on their ultrastructure characteristics (Strettoi et al., 1992). First, lobular appendages were counted in S1 to S3 proceeding from the INL toward the GCL. These synaptic endings were identified by their large size, pale matrix, and high density of synaptic vesicles (Figure 4A). Second, vitreal dendrites of type AII amacrine cells exhibiting an electron-dense, uniform matrix containing few synaptic vesicles were counted in S4 and S5 (Figure 4B). A total of 240 and 229 type AII amacrine endings (lobular appendages and dendrites) were quantified in control and *reeler*, respectively. The appearance of syn-

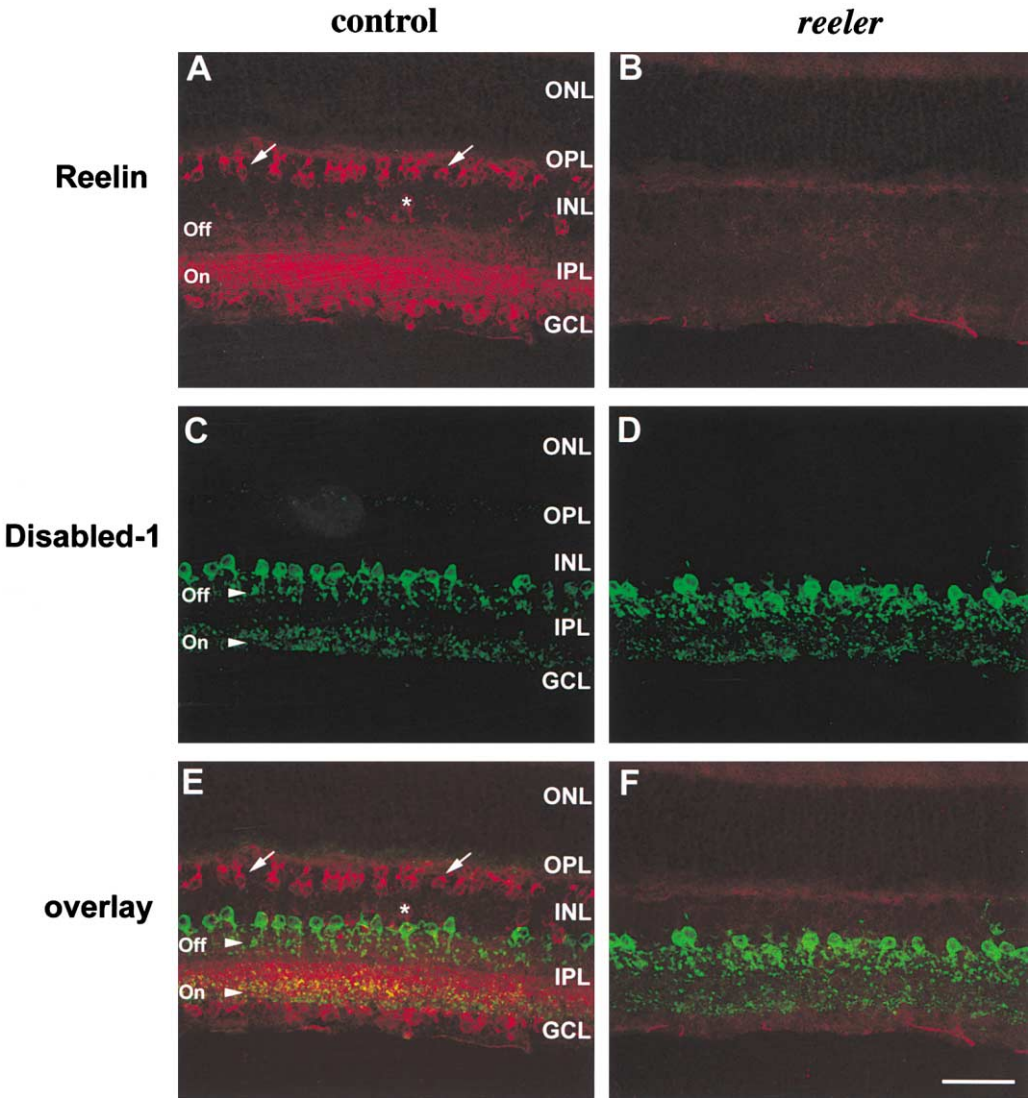

Figure 3. Distribution of Reelin and Dab1 in the Adult Eye

(A) Reelin is expressed in several populations of retinal cells. Reelin is present in the ganglion cell layer (GCL) and in the On sublayer of the IPL, which may represent dendrites of On retinal ganglion cells. Two different populations of cells in the inner nuclear layer (INL) contain Reelin, including bipolar cells (arrows) and amacrine cells (asterisk). (B) *Reeler* mice do not exhibit any specific staining with Reelin antibodies. (C) Dab1 is expressed in type AII amacrine cells in the INL. Their processes extend in the IPL, where they distribute into the On and Off sublayers (arrowheads). (D) In *reeler*, type AII amacrine cells are located in the correct cell layer, but the distribution of their processes is less precise compared to control. (E) In control, Reelin and Dab1 colocalize in the On sublayer of the IPL. Amacrine cells that contain Reelin (asterisk) do not express Dab1. (F) In *reeler*, the patterning of type AII amacrine cell endings in the IPL is less precise compared to that in control. The scale bar in (F) is 50 μm.

aptic endings was similar in both groups. The average number of AII endings in S1–S5 of control and *reeler* are shown in Figure 5A. Approximately 59% (82/138) of all lobular appendages in control retinas were located in S1 compared to 40% (60/150) in *reeler*. The paucity of appendages in S1 of *reeler* was compensated by a significant increase in both S2 and S3. The total number of type AII dendrites encountered in S4 and S5 was 102 in controls, compared to 79 in *reeler*. This is attributable to a significant reduction in the number of dendrites in S5 in *reeler* (Figure 5A). The average number of dendrites in control S5 was 5.8 ± 0.5, compared to 3.3 ± 0.4 (SEM) dendrites in *reeler* ($P = 0.002$).

Alterations in the distribution of type AII amacrine cell endings in IPL may reflect a change in the density of these neurons in the INL. Whole-mount preparations of retinas stained with Dab1 antibodies were used to determine the density of type AII amacrine cells in control and *reeler* mice. In control retinas ($n = 4$), the average density of AII amacrine cells was 3,333 ± 33 cells/mm^2 (Figure 5B). The density of these cells in *reeler*, 3,298 ± 118 cells/mm^2 ($n = 4$), was not statistically different (Figure 5B). Moreover, the central to peripheral ratio of type AII amacrine cells was 1.3:1 in both control and *reeler*, respectively. These estimates are similar to those in C57BL/6J mice (Rice and Curran, 2000). Therefore,

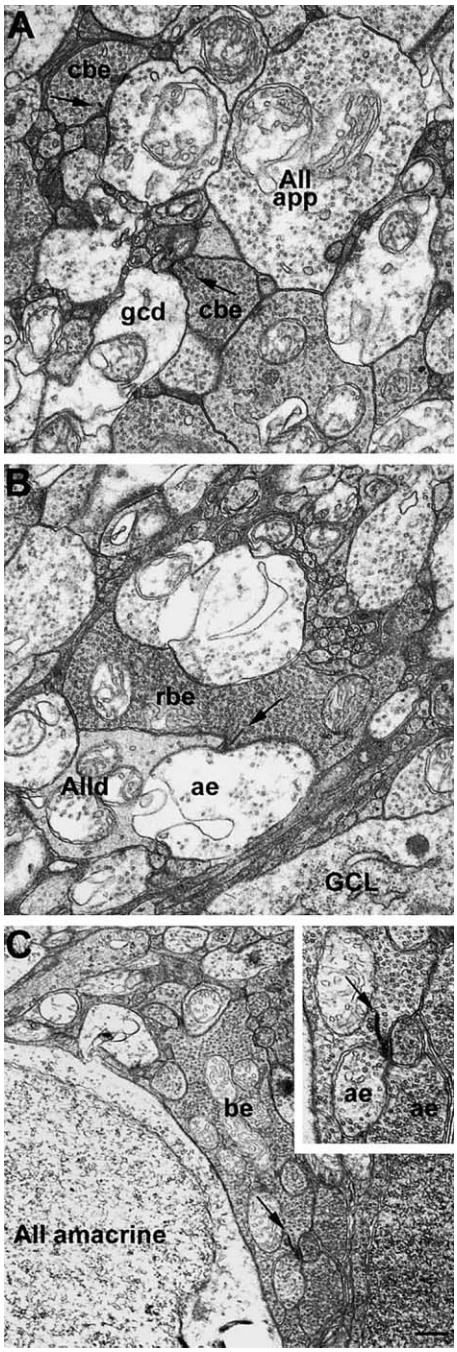

Figure 4. These Micrographs Illustrate the Ultrastructure Appearance of Synaptic Endings at Different Levels of the Inner Retina

Micrographs A and B are taken from control retinas. (A) Large, pale endings that are densely packed with synaptic vesicles are characteristic of the lobular appendages (AII app) of type AII amacrine cells that are located in S1–S3 of the IPL. Cone bipolar endings (cbe) contain numerous synaptic vesicles and synaptic ribbons (arrows). The cbe are postsynaptic to lobular appendages and presynaptic to ganglion cell dendrites (gcd). (B) The synaptic terminals of rod bipolar cells (rbe) are located in S5 of the IPL, near the GCL. The arrow indicates the synaptic ribbon of a rod bipolar cell terminal. The rbe are larger than cone bipolar cell terminals and they form a dyad synapse with two different amacrine cell endings. Dendrites originating from type AII amacrine cells (AIId) are electron dense and contain few vesicles. The other amacrine ending (ae) contains a pale matrix and many synaptic vesicles that make a reciprocal synapse with the rbe. These are amacrine cells that contain GABA as their primary neurotransmitter. (C) This micrograph taken from a *reeler* retina shows the cell body of a type AII amacrine cell juxtaposed to a very large bipolar ending (be) that resembles a rod bipolar cell ending. The arrow indicates the synaptic ribbon. The postsynaptic endings to this ribbon synapse contain many synaptic vesicles, indicating that these are amacrine cell endings (ae in inset) that do not resemble type AII dendrites. The scale bar in (C) is 0.3 μm in (A) and (B) and 0.5 μm in (C).

the abnormal distribution of synaptic endings originating from type AII amacrine cells in *reeler* is not explained by changes in density of these important interneurons in the absence of Reelin.

Type AII amacrine dendrites receive synaptic input from rod bipolar cells in S5 of the IPL (Famiglietti and Kolb, 1975). To determine if Reelin deficiency affects rod bipolar cells, adult retinas were double-labeled with antibodies recognizing Reelin and protein kinase C (PKC), a reliable marker for rod bipolar cells in mouse retina (Haverkamp and Wassle, 2000). Rod bipolar cells labeled with PKC did not contain Reelin (Figures 6A, 6C, and 6E). This result demonstrates that Reelin is present in a population of cone bipolar cells. In transverse sections, rod bipolar cells send a single axon to the IPL, where it terminates exclusively in the On sublamina (Figure 6C). In *reeler* mice, a subpopulation of rod bipolar axons stopped prematurely near the INL/IPL border (arrows in Figure 6D). The appearance of these "ectopic" terminals is reminiscent of the rod bipolar terminals normally located in the On sublamina of the IPL (Figure 6F). At the ultrastructural level, these terminals exhibited ribbon profiles, implying that they make functional synapses (inset in Figure 4C). These results indicate that Reelin deficiency affects the synaptic layering of rod bipolar cells and AII amacrine cells that contain Dab1.

Scrambler retinas were labeled with PKC antibodies to determine if Dab1 is required for proper synaptic organization of retinal interneurons. Whole-mount retinas and transverse sections were analyzed using confocal microscopy. In controls, rod bipolar cells were located in the middle of the retina and a single axon emerged from the cell body, projecting through the INL toward the IPL (Figure 7). (Rod bipolar axons branched at the level of the On sublamina in the IPL, where they terminated in several characteristic synaptic endings in S5, providing a uniform coverage of the retina surface [Figure 7C].) In both *reeler* and *scrambler*, rod bipolar cells were located in the correct layer and their axons traveled toward the IPL. However, ectopic terminals were present at the border between the INL and IPL (arrows in Figure 7B). This result indicates that both Reelin and Dab1 are required for normal synaptic organization in retina. Moreover, the apparent density of synaptic terminals was decreased in mice lacking Reelin or Dab1 compared to controls (Figure 7C).

Disruption of Reelin Signaling Results in a Decrease in Rod Bipolar Cells

In mice lacking Reelin or Dab1, the density of rod bipolar cells appeared decreased in either transverse retinal sections or whole-mount preparations (Figures 6 and 7). Whole-mount retina preparations were used to estimate

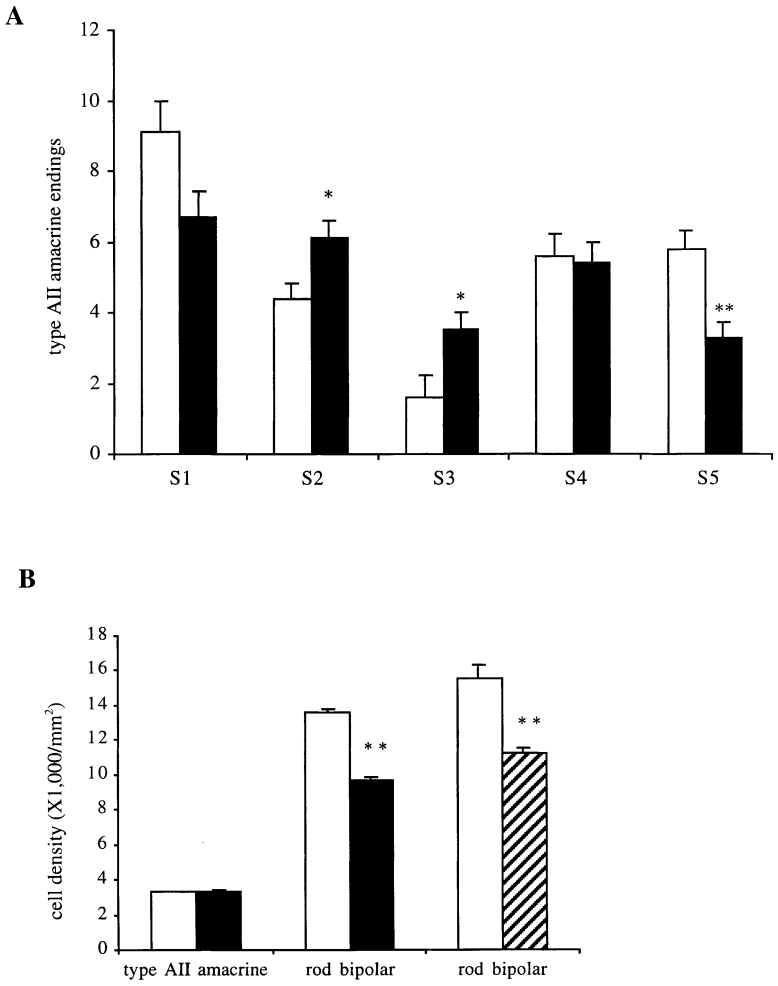

Figure 5. Deficiency in the Reelin Pathway Is Associated with an Alteration in the Distribution of Synaptic Endings in the IPL and a Reduction in Rod Bipolar Cell Density in the INL

(A) Distribution of synaptic endings originating from type AII amacrine cells in sublayers S1 to S5 in the IPL. Values represent the mean number of endings, analyzing an area of 43 μm^2 per sublayer. The majority of lobular appendages in control retinas (open bars) are present in S1. Their numbers decline in S2 and S3. In *reeler*, fewer lobular appendages are encountered in S1 compared to control. Their numbers in S2 and S3 are increased in *reeler* compared with control (*, $P < 0.05$). Type AII amacrine cell dendrites are present in equal numbers in S4 of control and *reeler*. However, the number of dendrites in S5 is significantly decreased in *reeler* (**, $P < 0.01$). (B) The density of type AII amacrine cells and rod bipolar cells in control, *reeler*, and mice lacking Dab1. The density of AII amacrine cells is similar in control (open) and *reeler* (black). However, rod bipolar cell density is decreased 29% in *reeler* compared with control. A similar decrease in rod bipolar cell density is apparent in mice lacking Dab1 (hatched) compared to their controls (**, $P < 0.01$). Error bars are ± SEM.

rod bipolar cell density at a comparable retinal eccentricity in control, *reelin*-, and *dab1*-deficient mice. The average density of rod bipolar cells was 13,550 ± 238 cells/mm² ($n = 5$) in control mice. The density in *reeler* mice was 9,659 ± 262 cells/mm² ($n = 6$), representing 29% fewer rod bipolar cells in the absence of Reelin (Figure 5B). A similar decrease (28%) is apparent when comparing control mice ($n = 3$) and mice lacking Dab1 ($n = 4$). Thus, despite the presence of Reelin, Dab1 deficiency results in fewer rod bipolar cells (Figure 5B). Therefore, both Reelin and Dab1 are required for the normal complement of rod bipolar cells to provide synaptic input to type AII amacrine cells.

ERG Responses Are Attenuated in the Absence of Reelin Signaling

Physiological responses in mice deficient in the Reelin pathway were determined using electroretinography (ERG). ERG responses were clearly detectable from both *reeler* and *scrambler* mice, but the responses were reduced in amplitude and the timing of peak components was frequently delayed compared to control mice. Representative ERGs for control, *reeler*, and *scrambler* are shown in Figure 8. Four different responses are shown for each group: a rod-mediated response to dim blue flash (rod-isolated response), a mixed rod and cone response to a bright white flash (maximal response), oscillatory potentials, and a cone response on a rod-saturating background. Summary descriptive statistics for each of these responses are given in Table 1.

Overall, the ERG results are consistent with disruption of the rod pathway in both *reeler* and *scrambler* mice. For example, the *b*-wave of the rod-isolated response (Figure 8) obtained from *reeler* mice was approximately half the amplitude of that in controls, and the implicit time (IT) of the *b*-wave peak was modestly delayed at 74.5 ms ($P = 0.0002$ and 0.013, for amplitude and implicit time, respectively). Summary parameters derived from the fit of the Naka-Rushton function to the blue intensity series also yielded a significantly reduced maximum saturated *b*-wave amplitude, V_{max}, in *reeler* mice (Table 1; $P < 0.001$). A similar pattern of responses was observed in *scrambler* mice (Table 1).

The response to a bright white flash (maximal response) is shown in the second column of Figure 8. Under dark-adapted conditions, the leading edge of the *a*-wave of the bright flash ERG is generally associated with rod photoreceptor activity (Granit, 1935, 1955; Penn and Hagins, 1969). The amplitude of the *a*-wave of the bright flash response was smaller in *reeler* mice, but the difference in the mean values of the *a*-wave in *reeler* and control mice was not significant ($P = 0.083$). This

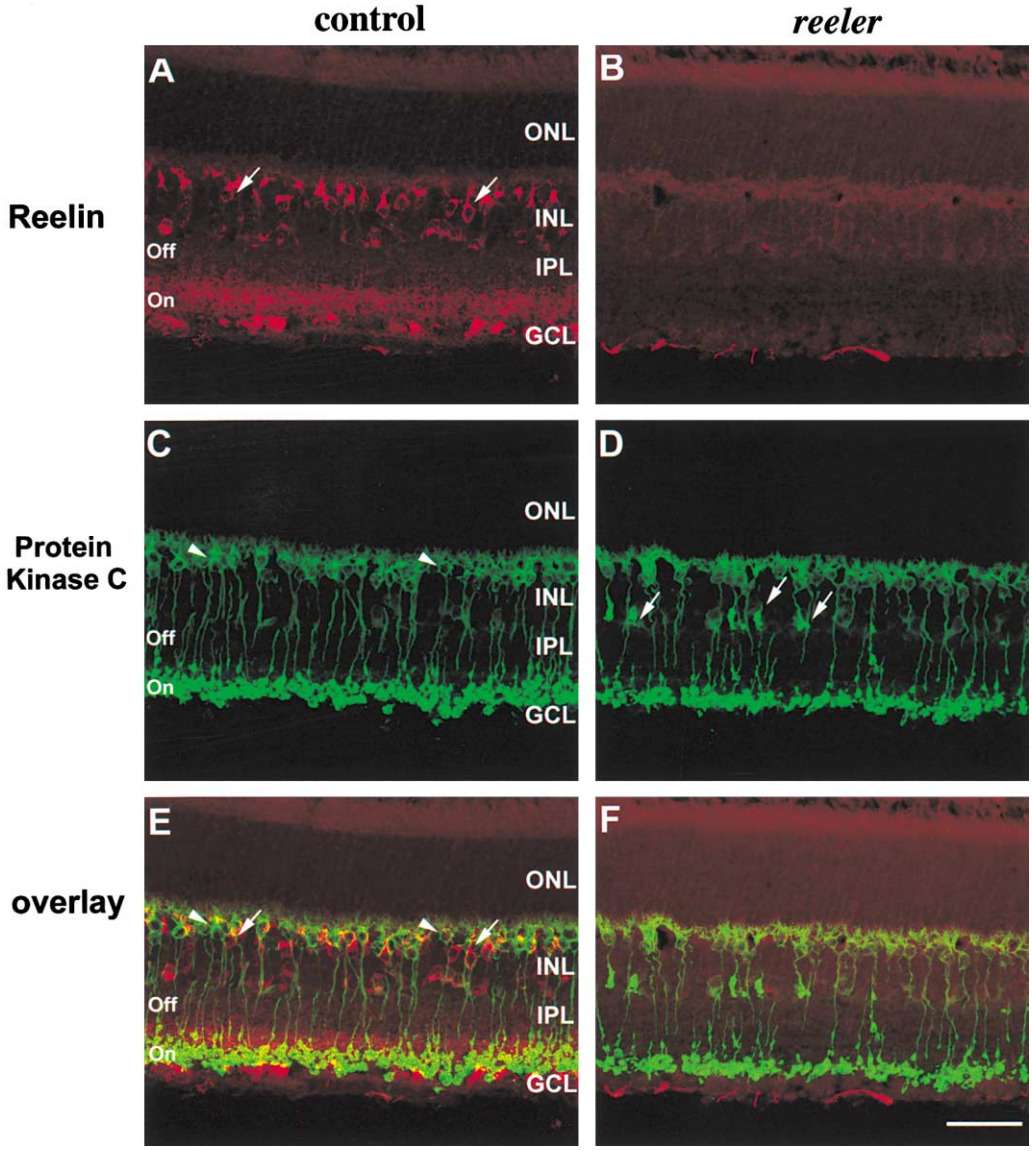

Figure 6. Distribution of Reelin and Protein Kinase C (PKC) in Adult Retina

(A) Reelin is expressed in the GCL and the On sublayer of the IPL. Reelin is also present in amacrine cells (not labeled) and bipolar cells, which extend dendrites (arrows) toward the outer nuclear layer (ONL). (B) *Reeler* mice do not exhibit any specific staining with Reelin antibodies. (C) PKC is expressed in rod bipolar cells, including their cell bodies (arrowheads) in the INL, dendrites, and axons that terminate in the On sublayer of the IPL. (D) In *reeler*, rod bipolar cells are located in the correct cell layer and the majority of axons reach the On sublayer of the IPL. However, a subpopulation of rod bipolar axons fails to reach this synaptic layer (arrows). (E) Bipolar cells expressing Reelin (arrows) are immunonegative for PKC (arrowheads), indicating that cone bipolar cells express Reelin. (F) The synaptic layering of rod bipolar cells is disrupted in the absence of Reelin. The scale bar in (F) is 50 μm.

implies that the photoreceptor function is relatively intact in *reeler*. In contrast to the *a*-wave, the *b*-wave of the bright flash response showed significant amplitude reductions (Table 1). On average, the amplitude of the *b*-wave in *reeler* was 0.33 log unit smaller than that for the control group ($P < 0.0001$). The rod *b*-wave of the ERG is generally associated with the combined activity of depolarizing rod bipolar cells and bipolar cell-dependent K^+ currents affecting Müller cells (Heynen and van Norren, 1985a, 1985b). The significantly reduced *b*-wave of the bright flash ERG is consistent with a disruption of the rod driven pathway in the inner retina in *reeler*. The larger deficits at the level of the inner retina in *reeler* were confirmed by the significantly smaller *a*- to *b*-wave amplitude ratio compared to controls ($P < 0.0001$). A similar pattern of results was observed in *scrambler* mice, although the functional deficits of the inner and outer retina appeared more uniform in this small cohort of animals.

The cellular origin of oscillatory potentials (OPs) is not completely understood, although they are likely generated by amacrine cells and other inner retinal cells interacting with bipolar and ganglion cells (Wachtmeister, 1998). Representative recordings of OPs are shown in

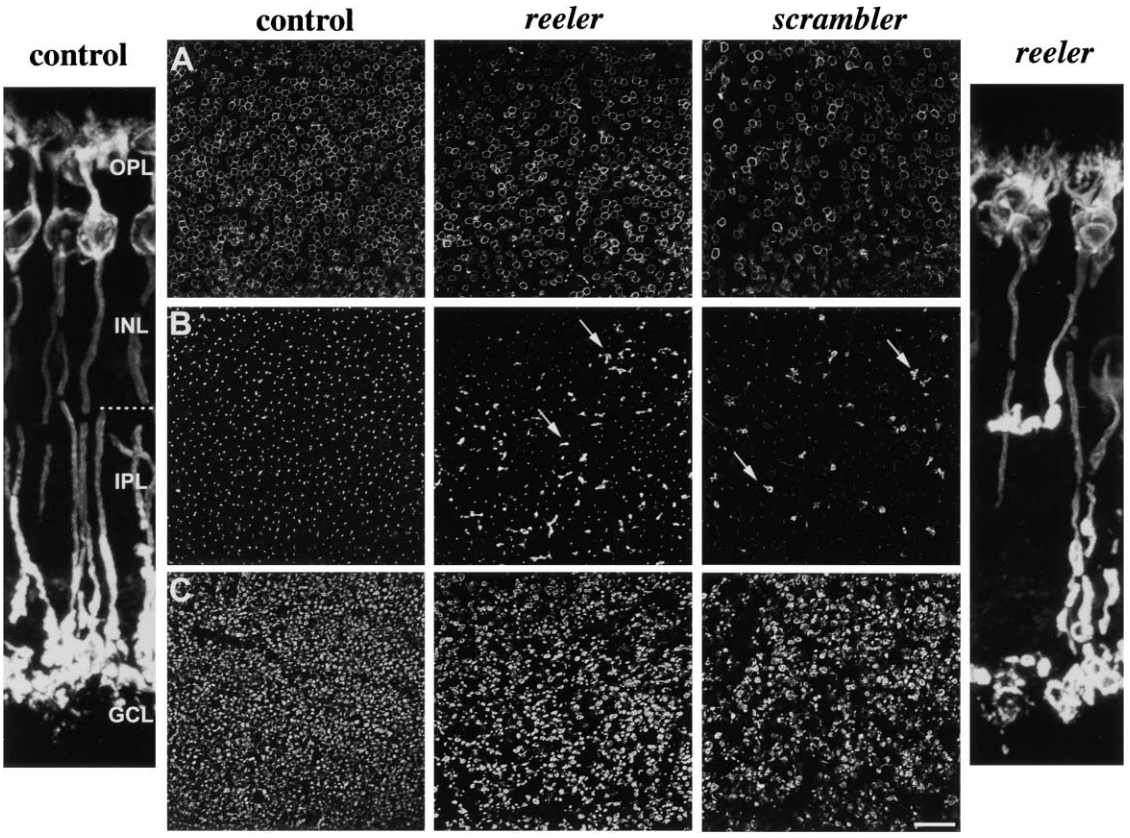

Figure 7. Rod Bipolar Cells Labeled with PKC Antibodies in Control, *reeler*, and *scrambler* Retinas

The micrographs on the left and right illustrate the appearance of these interneurons in cross-section of adult retinas. In control, cell bodies are located in the INL and their dendrites extend into the outer plexiform layer (OPL). Axons traverse the INL and IPL, where they terminate in S5 near the GCL. The hatched line indicates the border between the INL and IPL. Micrographs in (A)–(C) are taken at comparable levels at different depths in whole-mount retina preparations. (A) Rod bipolar cell bodies in control, *reeler*, and *scrambler* are present at similar positions within the INL. In both *reeler* and *scrambler*, there are fewer rod bipolar cells labeled with PKC. (B) Micrographs obtained from control mice reveal the axons of rod bipolar cells in cross-section. However, numerous rod bipolar terminals (arrows) appear at the border of the INL and IPL in both *reeler* and *scrambler*. Moreover, at the level of S5 in the IPL, there is a decrease in the density of rod bipolar terminals. In cross-sections of retina (right panel), these terminals stop at the level of the type AII amacrine cell bodies. The scale bar in (C) is 50 μm for (A)–(C) and 8 μm for the high magnification images on the left and right.

Figure 8. Four clearly defined oscillations were identifiable in the ERG recordings, hereafter referred to as OP1–OP4. Overall, OP amplitudes were significantly smaller ($F = 34.2$, df = 1/23, $P < 0.0001$) and delayed ($F = 19.9$, df = 1/23, $P = 0.0002$) in *reeler* compared to controls. The largest amplitude reductions occurred for OP1 and OP2, and the timing of positive deflections was progressively more delayed for the later OPs (Table 1). The OPs for the *scrambler* mice were also smaller and delayed. The diminished and delayed OPs in the *reeler* and *scrambler* mice are consistent with disruption of amacrine cell function or, alternatively, of the rod bipolar cell inputs.

Surprisingly, cone-mediated responses were reduced in amplitude and delayed in *reeler* compared to control mice ($P = 0.009$ and 0.007, for amplitude and implicit time, respectively). The cone ERG threshold (2.0 μV criterion) intensity was also modestly elevated ($P = 0.003$). However, the differences in cone function between *reeler* and control mice were smaller than those observed for rod function. For example, rod-isolated responses were on average 0.29 log units smaller in *reeler* compared to control mice, whereas cone responses were 0.17 log units smaller. Again, a similar pattern of results was observed in *scrambler* mice.

Discussion

Analysis of the neural retina in mice lacking either *reelin* or *dab1* has revealed an important role for these genes in the organization of synaptic connections. Reelin is expressed in three different cell types including retinal ganglion cells, amacrine cells, and cone bipolar cells. Failure to receive a Reelin-induced signal from one or more of these sources leads to the accumulation of Dab1. Reelin deficiency also results in an alteration in the distribution of synaptic endings originating from rod bipolar cells and type AII amacrine cells. The latter may explain the subtle alteration in the staining pattern of glycinergic amacrine cell processes in the IPL of Dab1-deficient retinas (Rice and Curran, 2000). Moreover, lack of either Reelin or Dab1 attenuates the rod-driven responses in the retina, as revealed by ERG analysis. Given the fact that *reelin*, *vldlr*, *apoER2*, and *dab1* con-

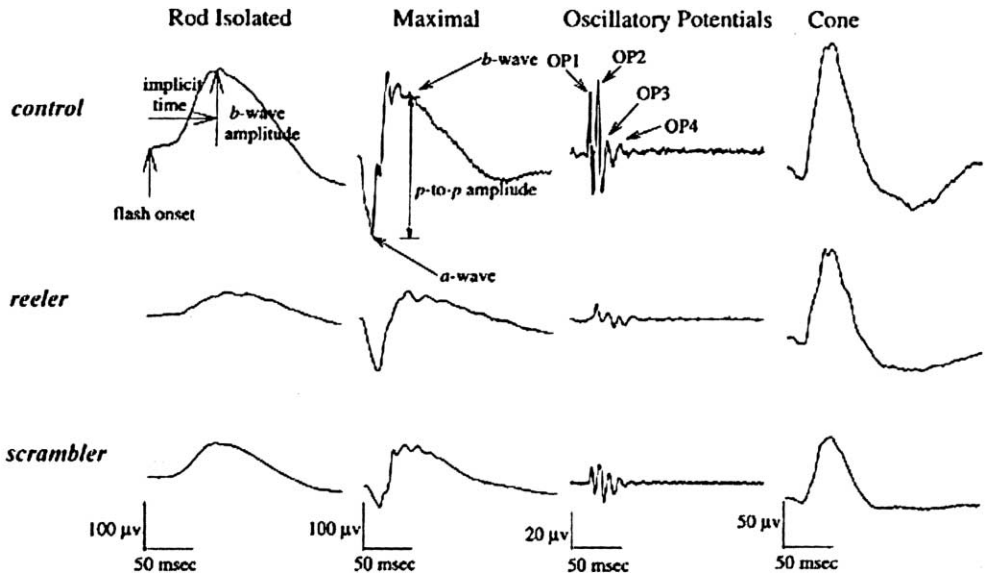

Figure 8. Representative Electroretinograph Responses Obtained from Control, *reeler*, and *scrambler* Mice

Shown from left to right are a rod-mediated response to a dim blue flash, a mixed rod and cone response to bright white flash, oscillatory potentials, and a cone-mediated response on a rod-suppressing background. Amplitude and timing calibrations are shown at the bottom of each set of graphs.

tinue to be expressed following neuronal migration (Kim et al., 1996; Alcantara et al., 1998; Rice et al., 1998), our results imply that another function of the Reelin pathway is to modulate the structure and function of retinal synaptic circuitry.

Rod bipolar cells are perhaps the most severely affected neuronal population in retinas of mice lacking Reelin or Dab1. The density of these cells, as determined using PKC as a marker, is decreased approximately 25%–30% in either *reelin* or *dab1* mutants compared to controls. The ERG demonstrated significant reductions in rod *b*-wave amplitudes, a finding that is consistent with the reduced rod bipolar cell counts. Rod bipolar cells receive synaptic input from rod photoreceptors and they provide excitatory synaptic output to the On sublayer of the IPL (Wässle et al., 1991). The primary synaptic targets of rod bipolar cells are amacrine cells, one of which corresponds to dendrites of type AII amacrine cells (Kolb and Famiglietti, 1974; Strettoi et al., 1990). While the density of type AII amacrine cells is indistinguishable in *reeler* and control, the number of dendrites in the On sublayer of the IPL is decreased in *reeler*. In addition, the ERG analysis demonstrated increasing functional deficits as signals were passed along the rod neural circuitry, particularly in the inner retina. Thus, while rod photoreceptor function was relatively normal in *reeler* mice, rod bipolar cell function was significantly reduced, and the output of amacrine cells, as reflected in the oscillatory potentials, was even further compromised (see Table 1).

The anatomical defects in rod bipolar cells and AII amacrine cells in the reeler retina cannot be interpreted in terms of a simple model. While it is formally possible that the alterations in these cell types arise independently, we favor the more parsimonious explanation in which both lesions result from an intrinsic defect in AII amacrine cells. In this scenario, a subpopulation of rod bipolar cells would be eliminated in the absence of either Reelin or Dab1 because they failed to make appropriate synaptic connections with the defective AII amacrine cells in the IPL. Amacrine cells differentiate during the first postnatal week in the mouse prior to the appearance of ribbon synapses in the IPL (Fisher, 1979; Young, 1985) (Rice and Curran, 2000). Type AII amacrine cell projections containing Dab1 encounter Reelin in the IPL during the period in which they elaborate processes in the On and Off sublayers establishing synaptic connections with rod bipolar cells (Fisher, 1979). We observed a defect in the patterning of type AII amacrine cell processes in the IPL at P7, whereas defects in the projections of rod bipolar cells were not apparent until P12 (data not shown). In adult *reeler* retinas, the number of type AII amacrine cell dendrites is decreased. Presumably, a deficiency in postsynaptic amacrine cell dendrites during circuit formation deprives a subset of rod bipolar axons of trophic factors that are critical for their survival. This explanation is consistent with the decrease in cell density of interneurons that occurs following depletion of ganglion cells around the time of birth (Gunhan-Agar et al., 2000; Williams et al., 2001). However, we cannot rule out the alternative explanation that a deficiency in the Reelin pathway could lead to a failure to produce the correct number of rod bipolar cells during neurogenesis. This, in turn, may affect the development of type AII amacrine cell dendrites during the first two postnatal weeks of retinal development. Regardless of the underlying mechanisms, the subtle alterations in the patterning of processes in the IPL implies that Reelin signaling, in combination with other cues such as neural activity, contributes to the development of synaptic connections that drive visual system function (Wong, 1999).

Table 1. Summary of ERG Response (±SD) in Control, *reeler*, and *scrambler* Mice

Rod-Isolated Response					
	b-Wave Amplitude	Implicit Time			
Control	129.8 (37.1)	67.8 (5.1)			
reeler	66.9 (34.2)	74.5 (7.4)			
scrambler	50.6 (17.5)	73.6 (4.0)			
Blue Intensity Series					
	V_{max}[a]	log *k*[b]	Threshold Intensity[c]		
Control	269.7 (52.8)	0.012 (0.016)	−4.18 (0.34)		
reeler	133.5 (48.2)	0.011 (0.017)	−4.05 (0.46)		
scrambler	117.8 (25.8)	0.012 (0.010)	−3.65 (0.27)		
Maximal Response[d]					
	a-Wave Amplitude	Implicit Time	*b*-Wave Amplitude	Implicit Time	*b*/*a*[e]
Control	69.7 (17.4)	17.1 (1.4)	285.7 (67.3)	39.9 (4.1)	4.2 (0.6)
reeler	56.2 (19.6)	21.9 (5.2)	134.0 (63.6)	52.4 (15.3)	2.4 (0.9)
scrambler	43.1 (23.5)	20.3 (1.2)	146.1 (45.8)	45.3 (2.3)	3.8 (1.5)
Oscillatory Potentials[f]					
	OP1		OP2		
	Amplitude	Implicit Time	Amplitude	Implicit Time	
Control	27.1 (9.2)	18.4 (2.4)	58.1 (25.6)	26.4 (3.1)	
reeler	9.2 (5.2)	23.8 (3.9)	11.9 (8.5)	35.2 (5.4)	
scrambler	8.2 (1.8)	21.9 (1.5)	13.3 (1.9)	31.5 (1.8)	
	OP3		OP4		
	Amplitude	Implicit Time	Amplitude	Implicit Time	
Control	35.9 (11.6)	35.3 (4.1)	15.8 (7.7)	47.7 (5.7)	
reeler	11.2 (7.1)	45.4 (8.3)	5.5 (3.0)	62.2 (10.7)	
scrambler	10.6 (2.2)	41.5 (1.8)	6.5 (1.8)	54.7 (2.5)	
Cone Response					
	Amplitude[g]	Implicit Time[h]	Threshold Intensity[i]		
Control	85.4 (25.0)	41.7 (3.0)	−1.18 (0.13)		
reeler	58.1 (21.0)	45.9 (3.9)	−0.98 (0.18)		
scrambler	56.4 (8.8)	44.8 (3.1)	−1.0 (0.10)		

[a,b] Parameters were derived from each of these intensity-response curves by fitting the best fit Naka-Rushton function: $V/V_{max} = I/(I + k)$, where V = rod peak-to-peak amplitude.
[c] log ERG threshold intensity = $\log k + 0.3 - \log(V_{max} - 2)$.
[d,f] Dark-adapted, white flashes = 8.46 cd-s/m^2.
[e] *b*-wave amplitude divided by *a*-wave amplitude.
[g,h] Light-adapted with 32.0 cd/m^2 background.
[i] Obtained by fitting linear regression to intensity-response series with slope constraint of 1.0.

In addition, in the absence of Reelin or Dab1, rod bipolar cells may exhibit synaptic plasticity and make inappropriate, but stable contacts with other neuronal elements. Indeed, we found that the ectopic rod bipolar terminals exhibit PKC immunoreactivity at the light microscopic level and synaptic ribbons at the ultrastructure level, suggesting that they likely represent functional connections. Other mutations that affect photoreceptors cause similar synaptic connectivity defects. For example, cones make ectopic synapses with rod bipolar cells when rod-specific genes such as *rhodopsin* or *cGMP phosphodiesterase* β*-subunit* are disrupted (Peng et al., 2000; Strettoi and Pignatelli, 2000). In addition, examples of neuritic "sprouting" have been documented in diseased human retinas and experimental models (Li et al., 1995; Lewis et al., 1998). Synaptic plasticity may be a common feature of abnormal visual function and, in the case of the Reelin pathway, compromised retinal micro-circuitry.

Accumulating evidence suggests that Reelin alters the adhesive properties of neurons. For example, aggregation assays demonstrated that neurons isolated from the *reeler* cortex are more adhesive than their normal counterparts (De Long and Sidman, 1970; Hoffarth et al., 1995; Ogawa et al., 1995). In the developing *reeler* hippocampal circuitry, entorhinal axons form abnormally tight bundles and exhibit both targeting errors and a decrease in collateral branching, suggesting that Reelin participates in the guidance mechanisms that control axonal growth (Del Rio et al., 1997; Borrell et al., 1999). One interpretation of these observations is that Reelin inhibits homotypic cell adhesion and axon fasciculation, thereby allowing neurons/axons to interact with

other cells or respond to additional extracellular cues. Reelin may trigger an intracellular signaling cascade that alters the surface properties of neurons containing Dab1, enabling them to recognize appropriate synaptic partners in retina. This may also be true in other brain regions that continue to express Reelin and Dab1. Therefore, in addition to its essential role during neuronal migration, the Reelin pathway may be important for the fine details and quantitative aspects of synaptic connections among neurons that form functional circuits.

Experimental Procedures

Animals

All animals were treated in accordance with institutional guidelines. B6C3H/J-*reeler* ^{2J} mice were obtained from the Jackson Laboratory (Bar Harbor, ME). All *reeler* mice used in this study were genotyped for the *rd* allele as described in Pittler et al. (1993). *Reeler* mice that contained either one or both copies of *rd* were excluded from physiological studies. *Scrambler* arose on the Dancer stock strain and it was subsequently outcrossed to C3H inbred mice, which fixed the *rd* allele in the genetic background of *scrambler* (Sweet et al., 1996). To obtain mice for physiological studies, *scrambler* was outcrossed to C57BL/6J and the resulting F1 mice were intercrossed to obtain *scrambler* mutants. Five *scrambler* homozygous mice were identified to have normal retinas based on fundoscopy.

Immunoblot Analysis of Retinas

Adult eyes were lysed with ice-cold buffer containing 50 mM Tris (pH = 7.4), 150 mM NaCl, 5 mM EDTA, 1% Triton-X, 10 μg/ml leupeptin, and 10 μg/ml aprotinin. Protein levels were measured using a protein assay kit (Bio-Rad, Richmond, CA). Approximately 100 μg of protein per lane was separated by using SDS-PAGE and transferred to a nitrocellulose membrane. A polyclonal antisera recognizing Dab1 (CT38) was used at a dilution of 1:3,000. Polyclonal antisera recognizing glutamate decarboxylase-67 (Chemicon) or Cdk5 were diluted to 1:5,000 and used as controls for protein loading. Following extensive washing, membranes were exposed to a 1:10,000 dilution of donkey anti-rabbit conjugated to horseradish peroxidase (Amersham). Enhanced chemiluminescence (Pierce Super Signal) was used to detect protein signals.

Expression Studies and Cell Density Estimates

Adult mice were deeply anesthetized with Avertin (0.2cc/10 g body weight) and perfused with 4% paraformaldeyhde in 0.1 M sodium phosphate buffered saline (PBS; pH = 7.2). Eyes were removed and processed either for cryosections or as whole-mount preparations. For cryosections, eyes were incubated in PBS-sucrose and embedded in tissue freezing medium (Triangle Biomedical Sciences, Durham, NC). Sections were cut at a thickness of 12–16 μm and mounted on Fisher Superfrost/Plus slides. Whole-mount retinal preparations were prepared as described previously (Rice and Curran, 2000). Primary antibodies were used at the following dilutions in 5% normal goat serum in PBS (Vector): mouse anti-Reelin G10 at 1:1,000, rabbit polyclonal antibody B3 anti-Dab at 1:1,000, and rabbit anti-protein kinase C at 1:2,000 (Cambio, UK). For double staining, primary antibodies were incubated together. Sections were incubated with either fluorescein conjugated goat anti-rabbit (Vector) or goat anti-mouse Alexa 594 (Molecular Probes, Eugene, OR) diluted at 1:200. Images were acquired using a Leica TCS confocal laser scanning microscope equipped with a 40× oil objective.

Whole-mount retinas immunostained with anti-Dab1 antibodies were used to determine the density of type AII amacrine cells in control (n = 4) and *reeler* (n = 4) mice. A total of 16 sample areas (10,000 μm^2) per retina was visualized using a 100× oil objective attached to a Leica confocal microscope. Eight sample areas located 0.5 mm from the retinal periphery and eight areas located 0.5 mm from the optic disc were analyzed per retina. Whole-mount retinas immunostained with protein kinase C antibodies were used to determine rod bipolar cell density in control (n = 5) and *reeler* (n = 6) mice. Mice deficient in Dab1 (n = 4) were compared to their control littermates (n = 3). Due to the poor antibody penetration in central retina, cell density estimates were obtained from eight sample areas per retina located 0.5 mm from the retinal periphery. Rod bipolar cells and AII amacrine cell density estimates are expressed at cells/mm^2. Statistical analysis was performed using the Student's t test.

Electron Microscopy

Six adult mice (3 control and 3 *reeler* Orleans) were anesthetized and perfused with 1% paraformaldehyde and 1% glutaraldehyde in 0.12 M phosphate buffer. Eyes were removed and the retinas were incubated in the same fixative overnight. Tissue was then post-fixed with 2% osmium tetroxide, stained with 2% uranyl acetate, and embedded in Araldite. Ultrathin sections from central retina were obtained and collected in formvar-coated slot grids and were subsequently stained with lead citrate. Serial micrographs covering the whole inner plexiform layer were taken at a magnification of 12,000×. Pictures were assembled into montages and the inner plexiform layer (IPL) was divided into five equally thick sublayers, named S1 to S5, proceeding from the inner nuclear layer (INL) to the ganglion cell layer (GCL) according to previous work in rabbits (Strettoi et al., 1990, 1992). Distances from the INL to the GCL were about 35 μm in control and *reeler*. The areas analyzed were approximately 43 μm^2 per sublayer. Nine to ten maps were analyzed in each sublayer of the IPL in control and *reeler* mice. Statistical analysis was performed using the Student's t test.

Electroretinography

Electroretinograms (ERGs) were performed on 30 adult mice (2 to 5 months of age). Descriptive statistics are provided for 14 control (5 +/+ and 9 +/−), 11 −/− *reeler*, and 5 *scrambler* mutant mice. All statistical comparisons are between control and *reeler* groups. Statistical analysis was performed using the Student's t test. The oscillatory potentials in control and *reeler* were compared using one-way analysis of variance (ANOVA). Following 2 hr of dark-adaptation, mice were anesthetized by intraperitoneal injection of 15 μg/gm Ketamine and 7 μg/gm xylazine in saline solution. ERGs were recorded from the corneal surface of one eye after pupil dilation (1% atropine sulfate) using a gold loop corneal electrode together with a mouth reference and tail ground electrode. Stimuli were produced with a Grass Photic Stimulator (PS33 Plus, Grass Instruments, Quincy, MA) affixed to the outside of a highly reflective Ganzfeld dome. Signals were amplified (10,000×, 1–1,000 Hz; CP511 AC amplifier, Grass Instruments), digitized (PCI-1200, National Instruments, Austin, TX), and computer-analyzed using custom software in a personal computer. Responses were computer-averaged with up to 100 records averaged for the weakest signals, and a signal rejection window was used to eliminate electrical artifacts. Flash presentation rate was 1 Hz, except at the highest intensities where flash frequency was slowed to avoid adaptation effects. Body temperature was monitored with a rectal probe and maintained at a constant temperature of 38°C.

Rod-mediated responses were recorded to short wavelength (Wratten 47A; λ_{max} = 470 nm) flashes of light flashes over a 1.0 log range of intensities (0.3 log unit steps) up to the maximum allowable by the photic stimulator (0.668 cd-s/m^2). Mixed rod and cone responses were obtained with white flashes incremented in 0.3 log unit steps up to the maximum allowable (8.46 cd-s/m^2). Oscillatory potentials were isolated using the same series of white flashes and a recording frequency range of 100–1000 Hz. Cone responses were recorded in response to an intensity series of white flashes (in 0.3 steps) on the rod-saturating background (32 cd/m^2). To analyze the rod-mediated responses to blue light, the intensity versus amplitude response curves were fitted to the Naka-Rushton function, $V/V_{max} = I/(I + k)$, where V = rod peak-to-peak amplitude, V_{max} = maximum rod amplitude, I = retinal illuminance, and k = retinal illuminance at half amplitude. The rod ERG threshold (2.0 μV criterion) was derived from the Naka-Rushton parameters, such that log threshold = log k + 0.3 − log(V_{max}−2). Similarly, the cone ERG threshold intensity (2.0 μV criterion) was derived from the fit of a linear regression (slope constraint of 1.0) to the intensity-response series obtained to white light on a rod-saturating background.

Acknowledgments

This work was supported by: NIH grants F32 EY06972 (D.S.R.), NIH Cancer Center Support CORE grant P30 CA21765, RO1 NS36558 (T.C.), the Human Frontiers Program RG67/98, grants SAF98-106 and 2FD1997-1760-C03-01 (E.S.) from the Spanish Ministery of Science and Technology, the American Lebanese Syrian Associated Charities (ALSAC), and The Foundation Fighting Blindness (SN). Special thanks to Drs. Brian Howell and André Goffinet for their generous gifts of rabbit anti-Dab1 (B3) and mouse anti-Reelin (G10) antibodies, respectively. Karen Forbes provided expert technical support and Norm Hawes (The Jackson Laboratory, Bar Harbor, ME) provided the out-crossed *scrambler* mice for physiological studies.

Received April 20, 2001; revised August 8, 2001.

References

Alcantara, S., Ruiz, M., D'Arcangelo, G., Ezan, F., de Lecea, L., Curran, T., Sotelo, C., and Soriano, E. (1998). Regional and cellular patterns of reelin mRNA expression in the forebrain of the developing and adult mouse. J. Neurosci. *18*, 7779–7799.

Borrell, V., Del Rio, J.A., Alcantara, S., Derer, M., Martinez, A., D'Arcangelo, G., Nakajima, K., Mikoshiba, K., Derer, P., Curran, T., and Soriano, E. (1999). Reelin regulates the development and synaptogenesis of the layer-specific entorhino-hippocampal connections. J. Neurosci. *19*, 1345–1358.

Caviness, V.S., Jr., and Rakic, P. (1978). Mechanisms of cortical development: a view from mutations in mice. Annu. Rev. Neurosci. *1*, 297–326.

D'Arcangelo, G., Miao, G.G., Chen, S.C., Soares, H.D., Morgan, J.I., and Curran, T. (1995). A protein related to extracellular matrix proteins deleted in the mouse mutant reeler. Nature *374*, 719–723.

D'Arcangelo, G., Homayouni, R., Keshvara, L., Rice, D.S., Sheldon, M., and Curran, T. (1999). Reelin is a ligand for lipoprotein receptors. Neuron *24*, 471–479.

De Long, G.R., and Sidman, R.L. (1970). Alignment deficit of reaggregating cells in culture of developing brains of reeler mutant mice. Dev. Biol. *22*, 584–600.

Del Rio, J.A., Heimrich, B., Borrell, V., Forster, E., Drakew, A., Alcantara, S., Nakajima, K., Miyata, T., Ogawa, M., Mikoshiba, K., et al. (1997). A role for Cajal-Retzius cells and reelin in the development of hippocampal connections. Nature *385*, 70–74.

Famiglietti, E.V., Jr., and Kolb, H. (1975). A bistratified amacrine cell and synaptic cirucitry in the inner plexiform layer of the retina. Brain Res. *84*, 293–300.

Fatemi, S.H., Earle, J.A., and McMenomy, T. (2000). Reduction in Reelin immunoreactivity in hippocampus of subjects with schizophrenia, bipolar disorder and major depression. Mol. Psychiatry *5*, 654–663.

Fisher, L.J. (1979). Development of synaptic arrays in the inner plexiform layer of neonatal mouse retina. J. Comp. Neurol. *187*, 359–372.

Goffinet, A.M. (1984). Events governing organization of postmigratory neurons: studies on brain development in normal and reeler mice. Brain Res. *319*, 261–296.

Granit, R. (1935). Two types of retinae and their electrical responses to intermittent stimuli in light and dark adaptation. J. Physiol. *85*, 421–438.

Granit, R. (1955). Receptors and Sensory Perception (New Haven: Yale University Press).

Guidotti, A., Auta, J., Davis, J.M., Gerevini, V.D., Dwivedi, Y., Grayson, D.R., Impagnatiello, F., Pandey, G., Pesold, C., Sharma, R., et al. (2000). Decrease in reelin and glutamic acid decarboxylase67 (GAD67) expression in schizophrenia and bipolar disorder: A postmortem brain study. Arch. Gen. Psychiatry *57*, 1061–1069.

Gunhan-Agar, E., Kahn, D., and Chalupa, L.M. (2000). Segregation of on and off bipolar cell axonal arbors in the absence of retinal ganglion cells. J. Neurosci. *20*, 306–314.

Haverkamp, S., and Wassle, H. (2000). Immunocytochemical analysis of the mouse retina. J. Comp. Neurol. *424*, 1–23.

Heynen, H., and van Norren, D. (1985a). Origin of the electroretinogram in the intact macaque eye—I. Principal component analysis. Vision Res. *25*, 697–707.

Heynen, H., and van Norren, D. (1985b). Origin of the electroretinogram in the intact macaque eye—II. Current source-density analysis. Vision Res. *25*, 709–715.

Hiesberger, T., Trommsdorff, M., Howell, B.W., Goffinet, A., Mumby, M.C., Cooper, J.A., and Herz, J. (1999). Direct binding of Reelin to VLDL receptor and ApoE receptor 2 induces tyrosine phosphorylation of disabled-1 and modulates tau phosphorylation. Neuron *24*, 481–489.

Hoffarth, R.M., Johnston, J.G., Krushel, L.A., and van der Kooy, D. (1995). The mouse mutation reeler causes increased adhesion within a subpopulation of early postmitotic cortical neurons. J. Neurosci. *15*, 4838–4850.

Hong, S.E., Shugart, Y.Y., Huang, D.T., Shahwan, S.A., Grant, P.E., Hourihane, J.O.B., Martin, N.D.T., and Walsh, C.A. (2000). Autosomal recessive lissencephaly with cerebellar hypoplasia is associated with human RELN mutations. Nat. Genet. *26*, 93–96.

Howell, B.W., Gertler, F.B., and Cooper, J.A. (1997a). Mouse disabled (mDab1): a Src binding protein implicated in neuronal development. EMBO J. *16*, 121–132.

Howell, B.W., Hawkes, R., Soriano, P., and Cooper, J.A. (1997b). Neuronal position in the developing brain is regulated by mouse disabled-1. Nature *389*, 733–737.

Howell, B.W., Herrick, T.M., and Cooper, J.A. (1999). Reelin-induced tyrosine phosphorylation of disabled 1 during neuronal positioning. Genes Dev. *13*, 643–648.

Howell, B.W., Herrick, T.M., Hildebrand, J.D., Zhang, Y.N., and Cooper, J.A. (2000). Dab1 tyrosine phosphorylation sites relay positional signals during mouse brain development. Curr. Biol. *10*, 877–885.

Keshvara, L., Benhayon, D., Magdaleno, S., and Curran, T. (2001). Identification of Reelin-induced sites of tyrosyl phosphorylation on Disabled-1. J. Biol. Chem. *276*, 16008–16014.

Kim, D.H., Iijima, H., Goto, K., Sakai, J., Ishii, H., Kim, H.J., Suzuki, H., Kondo, H., Saeki, S., and Yamamoto, T. (1996). Human apolipoprotein E receptor 2. A novel lipoprotein receptor of the low density lipoprotein receptor family predominantly expressed in brain. J. Biol. Chem. *271*, 8373–8380.

Kolb, H., and Famiglietti, E.V. (1974). Rod and cone pathways in the inner plexiform layer of cat retina. Science *186*, 47–49.

Lewis, G.P., Linberg, K.A., and Fisher, S.K. (1998). Neurite outgrowth from bipolar and horizontal cells after experimental retinal detachment. Invest. Ophthalmol. Vis. Sci. *39*, 424–434.

Li, Z.Y., Kljavin, I.J., and Milam, A.H. (1995). Rod photoreceptor neurite sprouting in retinitis pigmentosa. J. Neurosci. *15*, 5429–5438.

Lillien, L. (1994). Neurogenesis in the vertebrate retina. Persp. Dev. Neurobiol. *2*, 175–182.

Ogawa, M., Miyata, T., Nakajima, K., Yagyu, K., Seike, M., Ikenaka, K., Yamamoto, H., and Mikoshiba, K. (1995). The reeler gene-associated antigen on Cajal-Retzius neurons is a crucial molecule for laminar organization of cortical neurons. Neuron *14*, 899–912.

Peng, Y.W., Hao, Y., Petters, R.M., and Wong, F. (2000). Ectopic synaptogenesis in the mammalian retina caused by rod photoreceptor-specific mutations. Nat. Neurosci. *3*, 1121–1127.

Penn, R.D., and Hagins, W.A. (1969). Signal transmission along retinal rods and the origin of the electroretinographic a-wave. Nature *223*, 201–204.

Pittler, S.J., Keeler, C.E., Sidman, R.L., and Baehr, W. (1993). PCR analysis of DNA from 70-year-old sections of rodless retina demonstrates identity with the mouse rd defect. Proc. Natl. Acad. Sci. USA *90*, 9616–9619.

Rice, D.S., and Curran, T. (2000). Disabled-1 is expressed in type AII amacrine cells in the mouse retina. J. Comp. Neurol. *424*, 327–338.

Rice, D.S., Sheldon, M., D'Arcangelo, G., Nakajima, K., Goldowitz, D., and Curran, T. (1998). Disabled-1 acts downstream of Reelin in a signaling pathway that controls laminar organization in the mammalian brain. Development *125*, 3719–3729.

Schiffmann, S.N., Bernier, B., and Goffinet, A.M. (1997). Reelin mRNA

expression during mouse brain development. Eur. J. Neurosci. *9*, 1055–1071.

Sheldon, M., Rice, D.S., D'Arcangelo, G., Yoneshima, H., Nakajima, K., Mikoshiba, K., Howell, B.W., Cooper, J.A., Goldowitz, D., and Curran, T. (1997). Scrambler and yotari disrupt the disabled gene and produce a reeler-like phenotype in mice. Nature *389*, 730–733.

Sheppard, A.M., and Pearlman, A.L. (1997). Abnormal reorganization of preplate neurons and their associated extracellular matrix: an early manifestation of altered neocortical development in the reeler mutant mouse. J. Comp. Neurol. *378*, 173–179.

Strettoi, E., and Pignatelli, V. (2000). Modifications of retinal neurons in a mouse model of retinitis pigmentosa. Proc. Natl. Acad. Sci. USA *97*, 11020–11025.

Strettoi, E., Dacheux, R.F., and Raviola, E. (1990). Synaptic connections of rod bipolar cells in the inner plexiform layer of the rabbit retina. J. Comp. Neurol. *295*, 449–466.

Strettoi, E., Raviola, E., and Dacheux, R.F. (1992). Synaptic connections of the narrow-field, bistratified rod amacrine cell (AII) in the rabbit retina. J. Comp. Neurol. *325*, 152–168.

Sweet, H.O., Bronson, R.T., Johnson, K.R., Cook, S.A., and Davisson, M.T. (1996). Scrambler, a new neurological mutation of the mouse with abnormalities of neuronal migration. Mamm. Genome *7*, 798–802.

Trommsdorff, M., Gotthardt, M., Hiesberger, T., Shelton, J., Stockinger, W., Nimpf, J., Hammer, R.E., Richardson, J.A., and Herz, J. (1999). Reeler/Disabled-like disruption of neuronal migration in knockout mice lacking the VLDL receptor and ApoE receptor 2. Cell *97*, 689–701.

Wachtmeister, L. (1998). Oscillatory potentials in the retina: what do they reveal. Prog. Ret. Eye Res. *17*, 485–521.

Wässle, H., Yamashita, M., Greferath, U., Grunert, U., and Muller, F. (1991). The rod bipolar cell of the mammalian retina. Vis. Neurosci. *7*, 99–112.

Williams, R.R., Cusato, K., Raven, M.A., and Reese, B.E. (2001). Organization of the inner retina following elimination of the retinal ganglion cell population: effects on cell numbers and stratification patterns. Vis. Neurosci. *18*, 233–244.

Wong, R.O. (1999). Retinal waves and visual system development. Annu. Rev. Neurosci. *22*, 29–47.

Young, R.W. (1985). Cell differentiation in the retina of the mouse. Anat. Rec. *212*, 199–205.